PERGAMON

International Journal of Solids and Structures 39 (2002) 4583–4603

INTERNATIONAL JOURNAL OF SOLIDS and STRUCTURES

www.elsevier.com/locate/ijsolstr

Scattering of guided waves by circumferential cracks in composite cylinders

H. Bai [a], A.H. Shah [a], N. Popplewell [a], S.K. Datta [b,*]

[a] *Faculty of Engineering, University of Manitoba, Winnipeg, Manitoba, Canada R3T 2N2*
[b] *Department of Mechanical Engineering, University of Colorado, Boulder, CO 80309-0427, USA*

Received 3 February 2001; received in revised form 2 May 2002

Abstract

A somewhat generalized numerical procedure is used in this paper to study the problem of wave scattering by circumferential cracks in composite pipes. The study is motivated by the need to develop a model for the quantitative, ultrasonic non-destructive evaluation of cracks in pipes. For this purpose, a stiffness-based Rayleigh–Ritz type approach is employed first to obtain the approximate wave numbers and wave modes. Using the wave function expansions of the incident and scattered fields in the axial direction and decomposing the problem into separate symmetric and anti-symmetric problems, a three-dimensional wave scattering problem is reduced to two, independent two-dimensional problems over the circular cross-section. Both these problems can be reduced further to quasi-one-dimensions by discretizing the cross-section into finite elements and using a transfer matrix approach in the circumferential direction. This simplification greatly reduces the computational time. A comparison of the results for an isotropic pipe demonstrates the reliability and accuracy of the modified numerical procedure. Numerical results for the reflection and transmission coefficients of different incident wave modes are also presented for a 2-ply composite pipe with a crack. The crack may have an arbitrary circumferential length and radial depth. Simple extrapolations from one wave to another wave, separately incident on a crack, are demonstrated to be impossible due to different mode conversions by the crack.

Keywords: Ultrasonic scattering; Composite cylinder; Circumferential crack; Cylindrical orthotropy

1. Introduction

Metallic and composite circular tubes and pipelines are used extensively in the energy and transportation industries. Damage to these structures occurs due to handling, service load, natural disturbances, and environmental causes. Of particular interest to this study is the cracking that occurs in pipelines used

* Corresponding author. Fax: +1-303-492-3498.
E-mail address: dattas@spot.colorado.edu (S.K. Datta).

0020-7683/02/$ - see front matter
PII: S0020-7683(02)00339-6

in the oil, gas, and petrochemical industries. Ultrasonic non-destructive techniques are being developed for the inspection of such industrial pipelines. Ultrasonic waves in pipes can be generated quite efficiently by ring transducers (see Alleyne et al., 1998; Lowe et al., 1998) for launching waves that propagate along a pipe's axis. A major problem that is faced in the ultrasonic evaluation of pipes is the presence of a protective coating or insulation on the outside of the pipe wall. The coating or insulation material is much softer than the pipe's material and usually has a high wave attenuation. Access to the pipe from outside is difficult and various devices for access from inside the pipe have been under development. Also, ultrasonic waves propagating in the pipe wall can be modified by the coating or insulation layer. In a recent paper, Pan et al. (1999) examined the effect of a soft viscoelastic layer on guided ultrasonic waves in a bilayered plate. It was found that certain (Lamb wave) modes in a single layer steel plate are preferable for the inspection of damage because they do not suffer significant modification by the soft layer. Thus, mode selection plays a very important role in the success of ultrasonic non-destructive evaluation (NDE) techniques.

Guided waves in cylindrical tubes are similar in nature to the ones in plates although many more modes are excited in tubes (Alleyne et al., 1998). This makes an appropriate mode selection very critical for the success of an ultrasonic technique for pipeline inspection. The problem is complicated further if there are large cracks in the pipe wall. Thus, it is important to have accurate theoretical studies of ultrasonic wave propagation and scattering in cylindrical tubes.

As shown in previous studies (Kohl et al., 1992; Rattanawangcharoen, 1993; Rattanawangcharoen et al., 1994, 1997; Zhuang et al., 1997), the hybrid method is effective for axisymmetric scattering problems. However, for the three-dimensional scattering problem considered by Alleyne et al. (1998), the hybrid or full finite element method entails considerable computational costs. The objective of the present study is to present a more efficient, combined analytical/numerical technique for the investigation of three-dimensional scattering in a cylindrical tube. The cylinder is assumed to be composed of cylindrically orthotropic, fiber-reinforced composite materials. In order to model scattering by a part or full circumferential crack located in a cross-section of the cylinder, the problem is subdivided into a symmetric and an anti-symmetric problem about the plane of the crack. In order to decompose the original problem, the material of the cylinder must have a plane of symmetry, for example $z = 0$ where z is the axial direction. This approach has been used by Zhuang et al. (1999) to compute the Green's function for a cylindrical shell. A similar approach was also taken in Bai et al. (2001) to study scattering by a planar crack in a homogeneous isotropic cylinder. References to other related work can be found in Bai et al. (2001). In the present study and Bai et al. (2001), the crack can have an arbitrary depth in the radial direction. The scattered wave fields are expressed as sums of admissible wave functions in the axial direction. The cross-section of the tube, in which the crack is located, is divided into six-node planar elements and boundary conditions appropriate for the symmetric and anti-symmetric problems are imposed on these elements. Using a transfer matrix approach, each problem can be simplified to a quasi-one-dimensional problem. Unlike the isotropic cylinder, however, analytical solutions for cylindrical orthotropic materials are not in closed form. Therefore, they are computed here by using a finite element procedure in the radial direction. It is interesting to note, on the other hand, that this additional procedure hardly changes the overall computational time.

The crack considered is an ideal mathematical crack occupying an area located in the plane $z = 0$. It can have an arbitrary length in the circumferential direction and an arbitrary depth in the radial direction. The geometry of the cylinder and crack is shown in Fig. 1. The objective of this study is to investigate, for the first time, the extent to which the length and depth of a circumferential crack introduces wave scattering in a composite pipe. Consequently, reflection and transmission coefficients are presented for a cracked, laminated composite cylinder and various incident wave modes. The principle of energy conservation is used to ensure the accuracy of the numerical computations.

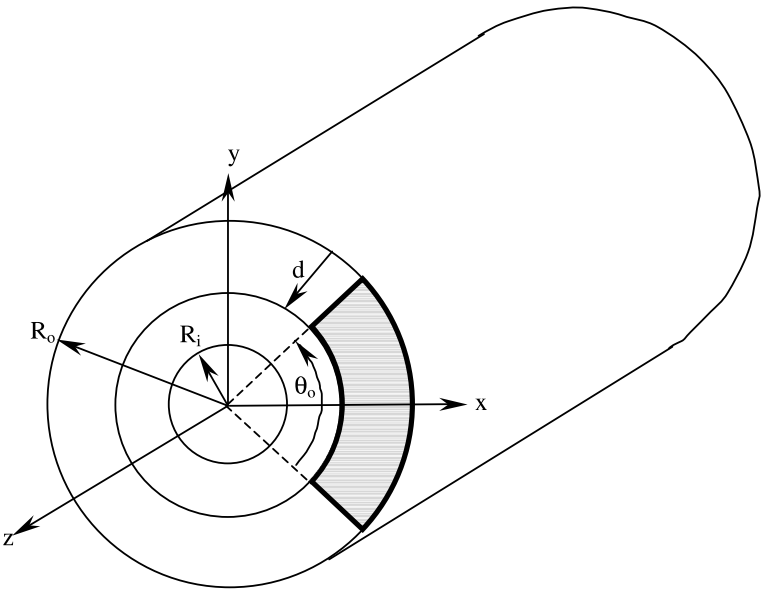

Fig. 1. Geometry of a composite cylinder. R_i: inner radius, R_o: outer radius, d: crack depth starting from cylinder's outer surface, θ_o: circumferential crack angle. The shadow region represents the crack.

2. Formulation

An infinitely long laminated circular cylinder is considered. The cylinder may be composed of layers or laminae having distinct mechanical properties and thicknesses. The circumferential crack, with arbitrary length and depth, is located at $z = 0$. The cylinder is discretized first through the thickness to model the radial inhomogeneity and to compute the wave numbers and corresponding wave functions. During the calculation of the reflection and transmission coefficients, the cylinder is discretized in both the circumferential, θ, and radial, r, directions over the cross-section $z = 0$. A time harmonic incident wave is generated at $z = +\infty$ that travels in the negative z-direction. It has an angular frequency ω and wave number ξ_{kl} in which k denotes the circumferential wave number and l is the axial wave mode. Because of the linearity of the governing equations and boundary conditions at $z = 0$, superposition can be used. The assumption of cylindrical orthotropicity implies that waves traveling in the positive and negative z-directions have the same wave numbers (Rattanawangcharoen et al., 1994). This assumption is needed for the symmetrical and anti-symmetrical decompositions to be valid. The displacement and traction components at the plane $z = 0$ can be arranged into two groups. One group involves the prescribed displacement components in the radial and circumferential directions as well as the prescribed traction component in the axial direction. The other group contains the axial displacement component and the traction components in the radial and circumferential directions. It can be shown that the quantities in the first group are known when the external forces are symmetric about the plane $z = 0$. On the other hand, quantities in the second group are known if the external forces are anti-symmetric about $z = 0$. In either case, only half the cylinder ($z \geqslant 0$) needs to be modeled. Using superposition of the solutions for the two individual problems, a complete solution can be constructed for the general three-dimensional case.

In the numerical procedure, a wave function expansion is used to represent the three dimensional, incident and scattered wave fields travelling in the axial direction. Then the displacement and traction

boundary conditions are satisfied in accordance with the symmetry and anti-symmetry conditions. Details can be found in Bai et al. (2001).

2.1. Wave modes

Consider the cylindrical coordinates (r, θ, z) where the origin is located at the center of the cylinder's cross-section (see Fig. 1). The displacement, strain, and stress components are defined as,

$$\vec{u}(r,\theta,z;t) = (u_r, u_\theta, u_z)^{\mathrm{T}}, \tag{1.1}$$

$$\vec{\varepsilon}(r,\theta,z;t) = (\varepsilon_{rr}, \varepsilon_{\theta\theta}, \varepsilon_{zz}, \gamma_{\theta z}, \gamma_{zr}, \gamma_{r\theta})^{\mathrm{T}} \tag{1.2}$$

and

$$\vec{\sigma}(r,\theta,z;t) = (\sigma_{rr}, \sigma_{\theta\theta}, \sigma_{zz}, \sigma_{\theta z}, \sigma_{zr}, \sigma_{r\theta})^{\mathrm{T}}. \tag{1.3}$$

Here, superscript 'T' represents the transpose. The general relation between the stress and strain components in a typical sublayer is,

$$\vec{\sigma} = D\vec{\varepsilon}, \tag{1.4}$$

where D is a 6 by 6 matrix of cylindrically orthotropic elastic moduli with the unique axis coinciding with the z-axis. The strain–displacement relation can be written as,

$$\vec{\varepsilon} = P_r \frac{\partial \vec{u}}{\partial r} + \frac{1}{r} P_\theta \frac{\partial \vec{u}}{\partial \theta} + P_z \frac{\partial \vec{u}}{\partial z} + \frac{1}{r} P_0 \vec{u}, \tag{1.5}$$

where

$$P_r = \begin{bmatrix} 1 & 0 & 0 \\ 0 & 0 & 0 \\ 0 & 0 & 0 \\ 0 & 0 & 0 \\ 0 & 0 & 1 \\ 0 & 1 & 0 \end{bmatrix}, \quad P_\theta = \begin{bmatrix} 0 & 0 & 0 \\ 0 & 1 & 0 \\ 0 & 0 & 0 \\ 0 & 0 & 1 \\ 0 & 0 & 0 \\ 1 & 0 & 0 \end{bmatrix}, \quad P_z = \begin{bmatrix} 0 & 0 & 0 \\ 0 & 0 & 0 \\ 0 & 0 & 1 \\ 0 & 1 & 0 \\ 1 & 0 & 0 \\ 0 & 0 & 0 \end{bmatrix}, \quad P_0 = \begin{bmatrix} 0 & 0 & 0 \\ 1 & 0 & 0 \\ 0 & 0 & 0 \\ 0 & 0 & 0 \\ 0 & 0 & 0 \\ 0 & -1 & 0 \end{bmatrix}. \tag{1.6}$$

Since the laminated cylinders are considered anisotropic and each lamina is a separate entity enjoying distinct mechanical properties and thickness, a Rayleigh–Ritz type approach is employed to approximate the wave number and functions. Details of the Rayleigh–Ritz type finite element method used can be found in Huang and Dong (1984) as well as in Datta (2000). Only a brief summary of the approach is presented here.

The displacement components, u_r, u_θ, and u_z, in the cylindrical coordinates, r, θ, and z, respectively, of the kth layer, which is bounded by r_k and r_{k+1}, are approximated by interpolation polynomials in the radial direction as,

$$\vec{u}(r,\theta,z;t) = N(\eta)\vec{q}(\theta,z;t), \tag{1.7}$$

with

$$r = n_1(\eta) r_k + n_2(\eta) r_m + n_3(\eta) r_{k+1}, \tag{1.8}$$

$$N(\eta) = \begin{bmatrix} n_1 & 0 & 0 & n_2 & 0 & 0 & n_3 & 0 & 0 \\ 0 & n_1 & 0 & 0 & n_2 & 0 & 0 & n_3 & 0 \\ 0 & 0 & n_1 & 0 & 0 & n_2 & 0 & 0 & n_3 \end{bmatrix}, \tag{1.9}$$

$$\vec{q}(\theta,z,t) = (u_{r1}, u_{\theta 1}, u_{z1}, u_{r2}, u_{\theta 2}, u_{z2}, u_{r3}, u_{\theta 3}, u_{z3})^{\mathrm{T}}. \tag{1.10}$$

In (1.7), the nodal displacements u_{rj}, $u_{\theta j}$, and u_{zj}, $j = 1, 2, 3$, are taken at the back (inner, $r = r_k$,), middle ($r = r_m$), and front (outer, $r = r_{k+1}$) surfaces of the sublayer, respectively. The interpolation polynomials, n_i, are quadratic functions given by,

$$n_1(\eta) = \tfrac{1}{2}(\eta^2 - \eta), \quad n_2(\eta) = 1 - \eta^2, \quad n_3(\eta) = \tfrac{1}{2}(\eta^2 + \eta), \quad -1 \leqslant \eta \leqslant 1. \tag{1.11}$$

By using Hamilton's principle, the governing equation is formulated for the entire cylinder as,

$$K_{zz}\frac{\partial^2 \vec{Q}}{\partial z^2} + K_{z\theta}\frac{\partial^2 \vec{Q}}{\partial z \partial \theta} + K_{\theta\theta}\frac{\partial^2 \vec{Q}}{\partial \theta^2} + K_z\frac{\partial \vec{Q}}{\partial z} + K_\theta\frac{\partial \vec{Q}}{\partial \theta} - K_r\vec{Q} - M\frac{\partial^2 \vec{Q}}{\partial t^2} = 0. \tag{1.12}$$

Here, K_{zz}, $K_{z\theta}$, $K_{\theta\theta}$, K_r, and M are real and symmetric whereas K_z and K_θ are real and anti-symmetric. The vector $\vec{Q}$ contains the nodal displacements along the radius in the cylinder.

A solution representing harmonic wave propagation for Eq. (1.12) can be assumed to take the form,

$$\vec{Q}(\theta, z, t) = \vec{Q}_0 e^{im\theta} e^{i(\xi z - \omega t)}, \tag{1.13}$$

where $\vec{Q}_0$ represents the nodal amplitude vector, $i = \sqrt{-1}$, ξ is the wave number in the z-direction, m is the circumferential wave number, and ω is the circular frequency. Substituting Eq. (1.13) into (1.12) results in the following set of linear homogeneous equations,

$$\left(-\xi^2 K_0 + i\xi K_1 - K_2\right)\vec{Q}_0 + \omega^2 M \vec{Q}_0 = 0, \tag{1.14}$$

where

$$K_0 = K_{zz}, \quad K_1 = imK_{z\theta} + K_z, \quad K_2 = m^2 K_{\theta\theta} - imK_\theta + K_r. \tag{1.15}$$

On the other hand, Eq. (1.14) provides the dispersion relation for the cylinder for a given value of frequency, ω. The quadratic algebraic eigenvalue problem (1.14) can be rearranged as,

$$\begin{bmatrix} 0 & I \\ \omega^2 M - K_2 & iK_1 \end{bmatrix} \begin{Bmatrix} \vec{Q}_0 \\ \xi \vec{Q}_0 \end{Bmatrix} = \xi \begin{bmatrix} I & \\ & K_0 \end{bmatrix} \begin{Bmatrix} \vec{Q}_0 \\ \xi \vec{Q}_0 \end{Bmatrix}. \tag{1.16}$$

The eigenvalues of the general eigenvalue problem (1.16) are the wave numbers, ξ. The upper half of the eigenvector corresponding to ξ is the wave function, $\vec{Q}_0$.

2.2. Modal expansion

The method detailed by Bai et al. (2001) is discussed briefly here. Assume that the incident wave field is generated at $z = +\infty$ and travels in the negative z-direction. Scattering (both reflection and transmission) occurs when the incident wave strikes the crack located at $z = 0$. The scattered wave field is composed of a finite number of propagating modes and an infinite number of non-propagating modes. Due to the symmetry and anti-symmetry about $z = 0$, only the reflected wave field needs to be evaluated in the positive z-direction. The displacements can be expanded as,

$$\begin{aligned}
u_r(\theta, z, t) &= \sum_{m=-M}^{M}\sum_{n=1}^{N_m} a_{kl,mn} u_{r,mn} e^{i\xi_{mn} z} e^{im\theta} e^{-i\omega t} = \sum_{m=-M}^{M} a_{kl,m} U_{r,m} E_m(z) e^{im\theta} e^{-i\omega t}, \\
u_\theta(\theta, z, t) &= \sum_{m=-M}^{M}\sum_{n=1}^{N_m} a_{kl,mn} u_{\theta,mn} e^{i\xi_{mn} z} e^{im\theta} e^{-i\omega t} = \sum_{m=-M}^{M} a_{kl,m} U_{\theta,m} E_m(z) e^{im\theta} e^{-i\omega t}, \\
u_z(\theta, z, t) &= \sum_{m=-M}^{M}\sum_{n=1}^{N_m} a_{kl,mn} u_{z,mn} e^{i\xi_{mn} z} e^{im\theta} e^{-i\omega t} = \sum_{m=-M}^{M} a_{kl,m} U_{z,m} E_m(z) e^{im\theta} e^{-i\omega t},
\end{aligned} \tag{2.1}$$

where

$$\begin{aligned} U_{r,m} &= \begin{pmatrix} u_{r,m1} & u_{r,m2} & \cdots & u_{r,mN_m} \end{pmatrix} \in \mathbf{C}^{\mathrm{NP}\times N_m}, \\ U_{\theta,m} &= \begin{pmatrix} u_{\theta,m1} & u_{\theta,m2} & \cdots & u_{\theta,mN_m} \end{pmatrix} \in \mathbf{C}^{\mathrm{NP}\times N_m}, \\ U_{z,m} &= \begin{pmatrix} u_{z,m1} & u_{z,m2} & \cdots & u_{z,mN_m} \end{pmatrix} \in \mathbf{C}^{\mathrm{NP}\times N_m}, \end{aligned} \tag{2.2}$$

$$u_{r,mj}, u_{\theta,mj}, u_{z,mj} \in \mathbf{C}^{\mathrm{NP}\times 1}, \quad j = 1, 2, \ldots, N_m, \tag{2.3}$$

$$a_{kl,m} = \begin{Bmatrix} a_{kl,m1} & a_{kl,m2} & \cdots & a_{kl,mN_m} \end{Bmatrix}^{\mathrm{T}} \in \mathbf{C}^{N_m\times 1} \tag{2.4}$$

and

$$E_m(z) = \mathrm{diag}\begin{bmatrix} \mathrm{e}^{\mathrm{i}\xi_{m1}z} & \mathrm{e}^{\mathrm{i}\xi_{m2}z} & \cdots & \mathrm{e}^{\mathrm{i}\xi_{mN_m}z} \end{bmatrix} \in \mathbf{C}^{N_m\times N_m}. \tag{2.5}$$

Here, NP is the number of nodal points in the radial direction and $a_{kl,mn}$ are unknown complex coefficients that are to be determined. The $u_{r,mj}$, $u_{\theta,mj}$ and $u_{z,mj}$ $(j = 1, 2, \ldots, N_m)$ are wave functions corresponding to the wave number, ξ_{mn}. N_m is the number of the axial wave mode corresponding to the circumferential wave number m. In $a_{kl,mn}$, the first two subscripts, k and l, indicate the wave numbers in the circumferential and axial directions, respectively, of the incident wave. The last two subscripts refer to the coefficients of the scattered wave fields corresponding to the wave numbers, m and n, in the circumferential and axial directions, respectively. The symbol $\boldsymbol{x} \in \mathbf{C}^{m\times n}$ means that $\boldsymbol{x}$ is a complex matrix of order m by n. It may be pointed out that the number of axial modes, N_m, need not be the same for different circumferential wave numbers, m. The factor $\mathrm{e}^{-\mathrm{i}\omega t}$ is suppressed for convenience in the sequel.

The stress components σ_{zr}, $\sigma_{z\theta}$ and σ_{zz} at the discrete nodal points of the kth sublayer can be obtained by using the stress–strain and strain–displacement relations. At each sublayer, the stress components also have a similar expansion as Eq. (2.1). Note that the stress components may not be continuous at the interfaces between the sublayers. With knowledge of the stresses, consistent nodal forces can be derived by using a standard procedure (see Bathe, 1982). The cross-section $z = 0$ is discretized into planar, nine-node quadrilateral elements.

2.3. Governing equations for the scattering problem

After decomposing the original problem into two separate problems, it is necessary to consider only half $(z \geqslant 0)$ the cylinder. Hence, only boundary conditions at the end $z = 0$ have to be satisfied. Because of the crack's existence in the cross-section, care must be taken on this part of the cross-section when dealing with the boundary conditions. Traction-free boundary conditions are imposed on the crack face for both the symmetric and anti-symmetric cases. Therefore, for the symmetric case, the boundary conditions are given by,

$$S = S^{\mathrm{I}} + S^{\mathrm{R}} = \begin{Bmatrix} S^{\mathrm{I}}_{\mathrm{C}} \\ S^{\mathrm{I}}_{\mathrm{N}} \end{Bmatrix} + \begin{Bmatrix} S^{\mathrm{R}}_{\mathrm{C}} \\ S^{\mathrm{R}}_{\mathrm{N}} \end{Bmatrix} = 0, \quad \text{at } z = 0, \tag{3.1}$$

with

$$S^{\mathrm{I}}_{\mathrm{C}} = \begin{Bmatrix} f^{\mathrm{I}}_r \\ f^{\mathrm{I}}_\theta \\ f^{\mathrm{I}}_z \end{Bmatrix}, \quad S^{\mathrm{I}}_{\mathrm{N}} = \begin{Bmatrix} f^{\mathrm{I}}_r \\ f^{\mathrm{I}}_\theta \\ u^{\mathrm{I}}_z \end{Bmatrix}, \quad S^{\mathrm{R}}_{\mathrm{C}} = \begin{Bmatrix} f^{\mathrm{R}}_r \\ f^{\mathrm{R}}_\theta \\ f^{\mathrm{R}}_z \end{Bmatrix}, \quad S^{\mathrm{R}}_{\mathrm{N}} = \begin{Bmatrix} f^{\mathrm{R}}_r \\ f^{\mathrm{R}}_\theta \\ u^{\mathrm{R}}_z \end{Bmatrix} \tag{3.2}$$

and, for anti-symmetry, they are,

$$A = A^{\mathrm{I}} + A^{\mathrm{R}} = \left\{ \begin{matrix} A^{\mathrm{I}}_{\mathrm{C}} \\ A^{\mathrm{I}}_{\mathrm{N}} \end{matrix} \right\} + \left\{ \begin{matrix} A^{\mathrm{R}}_{\mathrm{C}} \\ A^{\mathrm{R}}_{\mathrm{N}} \end{matrix} \right\} = 0, \quad \text{at } z = 0, \tag{3.3}$$

with

$$A^{\mathrm{I}}_{\mathrm{C}} = \left\{ \begin{matrix} f^{\mathrm{I}}_r \\ f^{\mathrm{I}}_\theta \\ f^{\mathrm{I}}_z \end{matrix} \right\}, \quad A^{\mathrm{I}}_{\mathrm{N}} = \left\{ \begin{matrix} u^{\mathrm{I}}_r \\ u^{\mathrm{I}}_\theta \\ f^{\mathrm{I}}_z \end{matrix} \right\}, \quad A^{\mathrm{R}}_{\mathrm{C}} = \left\{ \begin{matrix} f^{\mathrm{R}}_r \\ f^{\mathrm{R}}_\theta \\ f^{\mathrm{R}}_z \end{matrix} \right\}, \quad A^{\mathrm{R}}_{\mathrm{N}} = \left\{ \begin{matrix} u^{\mathrm{R}}_r \\ u^{\mathrm{R}}_\theta \\ f^{\mathrm{R}}_z \end{matrix} \right\}. \tag{3.4}$$

Here f_r, f_θ and f_z are the consistent nodal force components in the r, θ, and z-directions at the boundary $z = 0$, respectively. Superscripts 'I' and 'R' represent, respectively, the quantities associated with the incident and scattered wave fields. Subscripts 'C' and 'N' are used to denote a point in the cracked and uncracked region, respectively. Without loss of generality, the nodal sequence is assumed to be arranged such that the first P_{C} points are located in the cracked region. The remaining $P_{\mathrm{N}} = P - P_{\mathrm{C}}$ points are located in the uncracked region. It should be pointed out that Eqs. (3.1) and (3.3) are satisfied at each node that coincides with the boundary $z = 0$.

Consider, first, the symmetric case. It should be noted that when the mixed displacement and force components f_r, f_θ and u_z are known, the dual components u_r, u_θ and f_z are unknown for a point located in the uncracked region and vice versa. In the cracked region, all the force components are known and the corresponding dual displacement components are unknown.

At the cross-section $z = 0$, it is seen that

$$E_m(0) = \mathrm{diag}[\,1 \quad 1 \quad \cdots \quad 1\,] \in \mathbf{R}^{N_m \times N_m}. \tag{3.5}$$

The vectors $S^{\mathrm{R}}_{\mathrm{C}}$ and $S^{\mathrm{R}}_{\mathrm{N}}$ appearing in Eq. (3.1) may be written as,

$$S^{\mathrm{R}}_{\mathrm{C}} = G^{\mathrm{R}}_{\mathrm{C}} a, \qquad S^{\mathrm{R}}_{\mathrm{N}} = G^{\mathrm{R}}_{\mathrm{N}} a, \tag{3.6}$$

where

$$\begin{aligned} G^{\mathrm{R}}_{\mathrm{C}} &= [\, G^{\mathrm{R}}_{\mathrm{C},-M} \quad \cdots \quad G^{\mathrm{R}}_{\mathrm{C},m} \quad \cdots \quad G^{\mathrm{R}}_{\mathrm{C},M}\,] \in \mathbf{C}^{3P_{\mathrm{C}} \times N_{\mathrm{T}}}, \\ G^{\mathrm{R}}_{\mathrm{N}} &= [\, G^{\mathrm{R}}_{\mathrm{N},-M} \quad \cdots \quad G^{\mathrm{R}}_{\mathrm{N},m} \quad \cdots \quad G^{\mathrm{R}}_{\mathrm{N},M}\,] \in \mathbf{C}^{3P_{\mathrm{N}} \times N_{\mathrm{T}}}, \end{aligned} \tag{3.7}$$

$$a = \{\, a_{kl,-M} \quad \cdots \quad a_{kl,m} \quad \cdots \quad a_{kl,M}\,\}^{\mathrm{T}} \in \mathbf{C}^{N_{\mathrm{T}} \times 1} \tag{3.8}$$

and

$$G^{\mathrm{R}}_{\mathrm{C},m} = \begin{bmatrix} F^{\mathrm{R}}_{\mathrm{C},r,m} \\ F^{\mathrm{R}}_{\mathrm{C},\theta,m} \\ F^{\mathrm{R}}_{\mathrm{C},z,m} \end{bmatrix} \in \mathbf{C}^{3P_{\mathrm{C}} \times N_m}, \qquad G^{\mathrm{R}}_{\mathrm{N},m} = \begin{bmatrix} F^{\mathrm{R}}_{\mathrm{N},r,m} \\ F^{\mathrm{R}}_{\mathrm{N},\theta,m} \\ U^{\mathrm{R}}_{\mathrm{N},z,m} \end{bmatrix} \in \mathbf{C}^{3P_{\mathrm{N}} \times N_m}. \tag{3.9}$$

The total number of wave modes, N_{T}, considered in the wave function expansion is

$$N_{\mathrm{T}} = \sum_{m=-M}^{M} N_m, \tag{3.10}$$

where N_m corresponds to the axial mode involving the circumferential number m. The $a_{kl,m}$ is given by Eq. (2.4). The specific forms of matrices $F^{\mathrm{R}}_{\mathrm{C},r,m}$, $F^{\mathrm{R}}_{\mathrm{C},\theta,m}$, $F^{\mathrm{R}}_{\mathrm{C},z,m}$, $F^{\mathrm{R}}_{\mathrm{N},r,m}$, $F^{\mathrm{R}}_{\mathrm{N},\theta,m}$, and $U^{\mathrm{R}}_{\mathrm{N},z,m}$ are not given here as they can be found in Bai et al. (2001).

In a similar manner, the incident wave field, S^{I}, can be constructed as,

$$S^{\mathrm{I}}_{\mathrm{C}} = a^{\mathrm{I}}_{kl} g^{\mathrm{I}}_{\mathrm{C},kl}, \qquad S^{\mathrm{I}}_{\mathrm{N}} = a^{\mathrm{I}}_{kl} g^{\mathrm{I}}_{\mathrm{N},kl}. \tag{3.11}$$

Here, a^{I}_{kl} is the amplitude of the incident wave and $g^{\mathrm{I}}_{\mathrm{C},kl}$ is the vector obtained from the lth column of the matrix $G^{\mathrm{R}}_{\mathrm{C},k}$ by replacing each force component in the r- and θ-directions by its negative value. Similarly, vector $g^{\mathrm{I}}_{\mathrm{N},kl}$ is obtained from the lth column of matrix $G^{\mathrm{R}}_{\mathrm{N},k}$ by replacing each z direction force component by its negative value.

Eq. (3.1), see also Eq. (3.6), is solved by using the principle of virtual work. Then vectors $T^{\mathrm{R}}_{\mathrm{C}}$ and $T^{\mathrm{R}}_{\mathrm{N}}$, which are the dual components of the vectors $S^{\mathrm{R}}_{\mathrm{C}}$ and $S^{\mathrm{R}}_{\mathrm{N}}$, are formed as,

$$T^{\mathrm{R}} = \begin{Bmatrix} T^{\mathrm{R}}_{\mathrm{C}} \\ T^{\mathrm{R}}_{\mathrm{N}} \end{Bmatrix} = \begin{bmatrix} H^{\mathrm{R}}_{\mathrm{C}} \\ H^{\mathrm{R}}_{\mathrm{N}} \end{bmatrix} a, \tag{3.12}$$

with

$$T^{\mathrm{R}}_{\mathrm{C}} = \begin{Bmatrix} u^{\mathrm{R}}_{r} \\ u^{\mathrm{R}}_{\theta} \\ u^{\mathrm{R}}_{z} \end{Bmatrix}, \qquad T^{\mathrm{R}}_{\mathrm{N}} = \begin{Bmatrix} u^{\mathrm{R}}_{r} \\ u^{\mathrm{R}}_{\theta} \\ f^{\mathrm{R}}_{z} \end{Bmatrix} \tag{3.13}$$

and

$$\begin{aligned} H^{\mathrm{R}}_{\mathrm{C}} &= [\, H^{\mathrm{R}}_{\mathrm{C},-M} \quad \cdots \quad H^{\mathrm{R}}_{\mathrm{C},m} \quad \cdots \quad H^{\mathrm{R}}_{\mathrm{C},M} \,] \in \mathbf{C}^{3P_{\mathrm{C}} \times N_{\mathrm{T}}}, \\ H^{\mathrm{R}}_{\mathrm{N}} &= [\, H^{\mathrm{R}}_{\mathrm{N},-M} \quad \cdots \quad H^{\mathrm{R}}_{\mathrm{N},m} \quad \cdots \quad H^{\mathrm{R}}_{\mathrm{N},M} \,] \in \mathbf{C}^{3P_{\mathrm{N}} \times N_{\mathrm{CT}}}, \end{aligned} \tag{3.14}$$

$$H^{\mathrm{R}}_{\mathrm{C},m} = \begin{bmatrix} U^{\mathrm{R}}_{\mathrm{C},r,m} \\ U^{\mathrm{R}}_{\mathrm{C},\theta,m} \\ U^{\mathrm{R}}_{\mathrm{C},z,m} \end{bmatrix} \in \mathbf{C}^{3P_{\mathrm{C}} \times N_m}, \qquad H^{\mathrm{R}}_{\mathrm{N},m} = \begin{bmatrix} U^{\mathrm{R}}_{\mathrm{N},r,m} \\ U^{\mathrm{R}}_{\mathrm{N},\theta,m} \\ F^{\mathrm{R}}_{\mathrm{N},z,m} \end{bmatrix} \in \mathbf{C}^{3P_{\mathrm{N}} \times N_m}. \tag{3.15}$$

The specific form of the block matrices appearing in Eq. (3.15) can be found in Bai et al. (2001).

The principle of virtual work is applied by pre-multiplying the boundary conditions (3.1) by the dual components $T^{\mathrm{R}}_{\mathrm{C}}$ and $T^{\mathrm{R}}_{\mathrm{N}}$, so that,

$$\begin{bmatrix} H^{\mathrm{R}}_{\mathrm{C}} \\ H^{\mathrm{R}}_{\mathrm{N}} \end{bmatrix}^{*} \begin{bmatrix} G^{\mathrm{R}}_{\mathrm{C}} \\ G^{\mathrm{R}}_{\mathrm{N}} \end{bmatrix} a = -a^{\mathrm{I}}_{kl} \begin{bmatrix} H^{\mathrm{R}}_{\mathrm{C}} \\ H^{\mathrm{R}}_{\mathrm{N}} \end{bmatrix}^{*} \begin{Bmatrix} g^{\mathrm{I}}_{\mathrm{C},kl} \\ g^{\mathrm{I}}_{\mathrm{N},kl} \end{Bmatrix}. \tag{3.16}$$

The superscript $*$ denotes the complex conjugate plus matrix transpose.

The solutions of Eq. (3.16) give the reflection coefficients that are associated with the wave modes. Having found these coefficients, values of the displacement are readily obtained at different locations in the cylinder.

2.4. Reduction to quasi-one-dimensional problem

It should be noted that Eq. (3.16) is derived by using pointwise conditions. This is a computationally demanding procedure due to the large number of nodes of the two-dimensional mesh in the plane $z = 0$, as shown in Fig. 2. If a transfer matrix from radius to radius is considered, instead of a point to point transfer, calculations can be performed more efficiently. This idea is based upon the circular symmetry of the geometry and the physical characteristics of the problem (see expansion (3.1)).

Consider the two vectors $f_{\mathrm{C},r,mn} \in \mathbf{C}^{P_{\mathrm{C}} \times 1}$ and $f_{\mathrm{N},r,mn} \in \mathbf{C}^{P_{\mathrm{N}} \times 1}$, which are located in the nth column of the matrices $F^{\mathrm{R}}_{\mathrm{C},r,m}$ and $F^{\mathrm{R}}_{\mathrm{N},r,m}$. It should be noted that these two vectors are evaluated at all the nodes of the cracked and uncracked regions, respectively. First construct two vectors $f^{(1)}_{\mathrm{C},r,mn}$ and $f^{(1)}_{\mathrm{N},r,mn}$ that correspond to these two vectors. They are evaluated at the two adjacent radii $\theta = 0$ and $\theta = \pi/q$, where q is the number of subdivisions in the circumferential direction. Also, denote the two radii, $\theta = 2j\pi/q$ and $\theta = (2j+1)\pi/q$, for $j = 0, 1, \ldots, q-1$, as the jth radius pair in the following discussion. Without loss of generality, assume that q_{C} and q_{N} radii pairs are located in the cracked and uncracked regions, respectively. By considering the

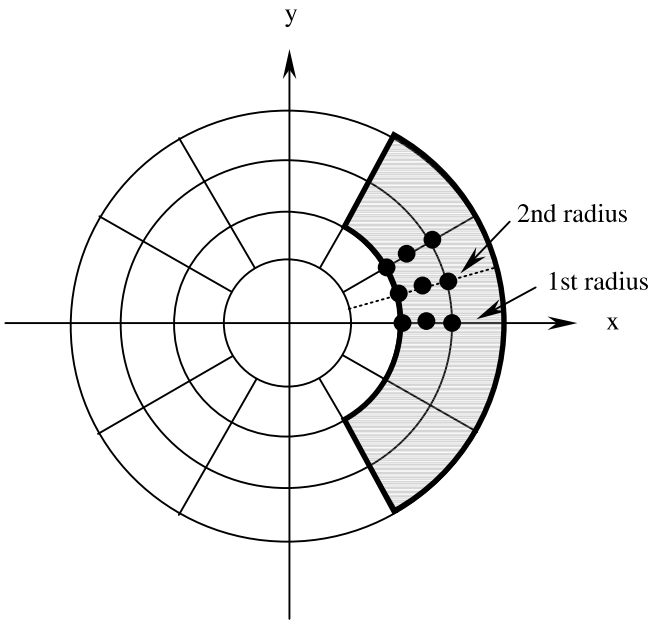

Fig. 2. A typical mesh in the cracked cross-section. The shadow region represents the crack.

wave functions in Eq. (2.1), it can be shown that the values of the two vectors, $f_{C,r,mn}$ and $f_{N,r,mn}$, on the jth radius pair can be obtained by a simple rotation, $e^{2imk\pi/q}$, of that on the first radius pair $f^{(1)}_{C,r,mn}$ and $f^{(1)}_{N,r,mn}$. Therefore,

$$f^{(j)}_{C,r,mn} = \lambda_m^{j-1} f^{(1)}_{C,r,mn}, \quad 1 \leqslant j \leqslant q_C, \tag{4.1}$$

$$f^{(j)}_{N,r,mn} = \lambda_m^{j-1} f^{(1)}_{N,r,mn}, \quad q_C + 1 \leqslant j \leqslant q = q_C + q_N, \tag{4.2}$$

where

$$\lambda_m = e^{2im\pi/q}. \tag{4.3}$$

Thus, the vectors $f_{C,r,mn}$ and $f_{N,r,mn}$ can be written more compactly as,

$$f_{C,r,mn} = \Lambda_{C,m} f^{(1)}_{C,r,mn}, \qquad f_{N,r,mn} = \Lambda_{N,m} f^{(1)}_{N,r,mn}, \tag{4.4}$$

with the transfer matrices $\Lambda_{C,m}$ and $\Lambda_{N,m}$, given by

$$\Lambda_{C,m} = \left\lfloor \widehat{I} \quad \lambda_m \widehat{I} \quad \cdots \quad \lambda_m^{q_C-1} \widehat{I} \right\rfloor^T \in \mathbf{C}^{2pq_C \times 2p} \tag{4.5}$$

and

$$\Lambda_{N,m} = \lambda_m^{q_C} \left\lfloor \widehat{I} \quad \lambda_m \widehat{I} \quad \cdots \quad \lambda_m^{q_N-1} \widehat{I} \right\rfloor^T \in \mathbf{C}^{2pq_N \times 2p}. \tag{4.6}$$

Here, $\widehat{I}$ is the unit matrix of order $2p$ where $2p$ is the total number of nodes in a radius pair. With the help of Eq. (4.4), the matrices $F^R_{C,r,m}$ and $F^R_{N,r,m}$ can then be expressed as

$$F^R_{C,r,m} = \Lambda_{C,m} F^{(1)R}_{C,r,m}, \qquad F^R_{N,r,m} = \Lambda_{N,m} F^{(1)R}_{N,r,m}. \tag{4.7}$$

The matrices $F^{(1)\mathrm{R}}_{\mathrm{C},r,m}$ and $F^{(1)\mathrm{R}}_{\mathrm{N},r,m}$ have similar forms to the original matrices $F^{\mathrm{R}}_{\mathrm{C},r,m}$ and $F^{\mathrm{R}}_{\mathrm{N},r,m}$ after changing each column with $f^{(1)}_{\mathrm{C},r,mn}$ and $f^{(1)}_{\mathrm{N},r,mn}$, respectively. Using these new expressions, the matrices $G^{\mathrm{R}}_{\mathrm{C}}$ and $G^{\mathrm{R}}_{\mathrm{N}}$ can be shown to have the following forms

$$G^{\mathrm{R}}_{\mathrm{C}} = \left[\widetilde{\Lambda}_{\mathrm{C},-M} G^{(1)\mathrm{R}}_{\mathrm{C},-M} \quad \cdots \quad \widetilde{\Lambda}_{\mathrm{C},m} G^{(1)\mathrm{R}}_{\mathrm{C},m} \quad \cdots \quad \widetilde{\Lambda}_{\mathrm{C},M} G^{(1)\mathrm{R}}_{\mathrm{C},M} \right], \tag{4.8}$$

$$G^{\mathrm{R}}_{\mathrm{N}} = \left[\widetilde{\Lambda}_{\mathrm{N},-M} G^{(1)\mathrm{R}}_{\mathrm{N},-M} \quad \cdots \quad \widetilde{\Lambda}_{\mathrm{N},m} G^{(1)\mathrm{R}}_{\mathrm{N},m} \quad \cdots \quad \widetilde{\Lambda}_{\mathrm{N},M} G^{(1)\mathrm{R}}_{\mathrm{N},M} \right], \tag{4.9}$$

where

$$\widetilde{\Lambda}_{\mathrm{C},m} = \begin{bmatrix} \Lambda_{\mathrm{C},m} & & \\ & \Lambda_{\mathrm{C},m} & \\ & & \Lambda_{\mathrm{C},m} \end{bmatrix} \in \mathbf{C}^{6pq_{\mathrm{C}} \times 6p} \tag{4.10}$$

and

$$\widetilde{\Lambda}_{\mathrm{N},m} = \begin{bmatrix} \Lambda_{\mathrm{N},m} & & \\ & \Lambda_{\mathrm{N},m} & \\ & & \Lambda_{\mathrm{N},m} \end{bmatrix} \in \mathbf{C}^{6pq_{\mathrm{N}} \times 6p}. \tag{4.11}$$

The block matrices $G^{(1)\mathrm{R}}_{\mathrm{C},m}$ and $G^{(1)\mathrm{R}}_{\mathrm{N},m}$ are obtained from $G^{\mathrm{R}}_{\mathrm{C},m}$ and $G^{\mathrm{R}}_{\mathrm{N},m}$ by replacing the corresponding force and displacement components with their reference vectors. The latter are evaluated only at the first radius pair. Similar relations hold also for the matrices $H^{\mathrm{R}}_{\mathrm{C}}$, $H^{\mathrm{R}}_{\mathrm{N}}$ and vectors $S^{\mathrm{I}}_{\mathrm{C}}$, $S^{\mathrm{I}}_{\mathrm{N}}$.

With the above simplification, it can be shown that

$$\left(H^{\mathrm{R}}_{\mathrm{C}}\right)^{*} G^{\mathrm{R}}_{\mathrm{C}} = \begin{bmatrix} \cdots & \cdots & \cdots \\ \cdots & \mu_{\mathrm{C},m_1 m_2} \left(H^{(1)\mathrm{R}}_{\mathrm{C},m_1}\right)^{*} G^{(1)\mathrm{R}}_{\mathrm{C},m_2} & \cdots \\ \cdots & \cdots & \cdots \end{bmatrix} \in \mathbf{C}^{N \times N}, \tag{4.12}$$

$$\left(H^{\mathrm{R}}_{\mathrm{N}}\right)^{*} G^{\mathrm{R}}_{\mathrm{N}} = \begin{bmatrix} \cdots & \cdots & \cdots \\ \cdots & \mu_{\mathrm{N},m_1 m_2} \left(H^{(1)\mathrm{R}}_{\mathrm{N},m_1}\right)^{*} G^{(1)\mathrm{R}}_{\mathrm{N},m_2} & \cdots \\ \cdots & \cdots & \cdots \end{bmatrix} \in \mathbf{C}^{N \times N}, \tag{4.13}$$

$$\left(H^{\mathrm{R}}_{\mathrm{C}}\right)^{*} S^{\mathrm{I}}_{\mathrm{C}} = \begin{Bmatrix} \vdots \\ \mu_{\mathrm{C},mk} \left(H^{(1)\mathrm{R}}_{\mathrm{C},m}\right)^{*} g^{(1)\mathrm{R}}_{\mathrm{C},kl} \\ \vdots \end{Bmatrix} \in \mathbf{C}^{N \times 1}, \tag{4.14}$$

$$\left(H^{\mathrm{R}}_{\mathrm{N}}\right)^{*} S^{\mathrm{I}}_{\mathrm{N}} = \begin{Bmatrix} \vdots \\ \mu_{\mathrm{N},mk} \left(H^{(1)\mathrm{R}}_{\mathrm{N},m}\right)^{*} g^{(1)\mathrm{R}}_{\mathrm{N},kl} \\ \vdots \end{Bmatrix} \in \mathbf{C}^{N \times 1} \tag{4.15}$$

and

$$\mu_{\mathrm{C},m_1 m_2} = \begin{cases} q_{\mathrm{C}}, & \text{for } m_1 = m_2, \\ \dfrac{1 - \lambda^{q_{\mathrm{C}}}_{m_1,m_2}}{1 - \lambda_{m_1,m_2}}, & \text{for } m_1 \neq m_2, \end{cases} \tag{4.16}$$

$$\mu_{\mathrm{N},m_1m_2} = \begin{cases} q_{\mathrm{N}}, & \text{for } m_1 = m_2, \\ -\dfrac{1-\lambda_{m_1,m_2}^{q_C}}{1-\lambda_{m_1,m_2}}, & \text{for } m_1 \neq m_2, \end{cases} \tag{4.17}$$

$$\lambda_{m_1,m_2} = \lambda_{m_1}^{*}\lambda_{m_2} = \mathrm{e}^{2\mathrm{i}(m_2-m_1)\pi/q}. \tag{4.18}$$

Eqs. (4.16) and (4.17) may also be written as

$$\mu_{\mathrm{C},m_1m_2} + \mu_{\mathrm{N},m_1m_2} = q\delta_{m_1m_2}, \tag{4.19}$$

where

$$\delta_{m_1m_2} = \begin{cases} 1, & \text{for } m_1 = m_2, \\ 0, & \text{for } m_1 \neq m_2. \end{cases} \tag{4.20}$$

Substituting Eqs. (4.12)–(4.15) into Eq. (3.16) results in the final equation,

$$\left[\left(H_{\mathrm{C}}^{\mathrm{R}}\right)^{*}G_{\mathrm{C}}^{\mathrm{R}} + \left(H_{\mathrm{N}}^{\mathrm{R}}\right)^{*}G_{\mathrm{N}}^{\mathrm{R}}\right]a = -a_{kl}^{\mathrm{I}}\left[\left(H_{\mathrm{C}}^{\mathrm{R}}\right)^{*}S_{\mathrm{C}}^{\mathrm{I}} + \left(H_{\mathrm{N}}^{\mathrm{R}}\right)^{*}S_{\mathrm{N}}^{\mathrm{I}}\right]. \tag{4.21}$$

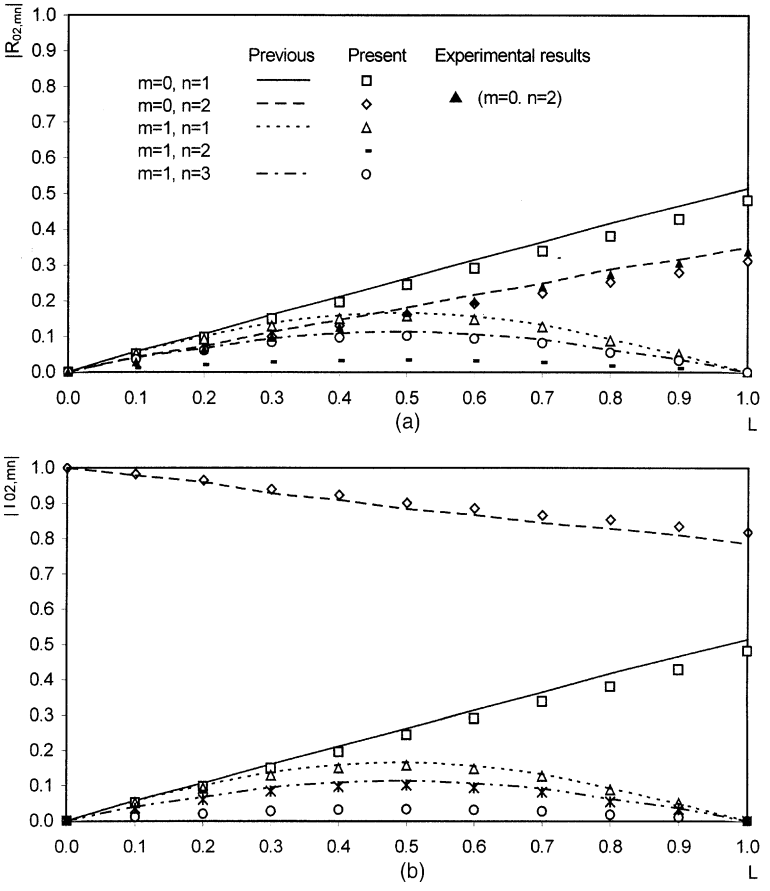

Fig. 3. Reflection and transmission coefficients, $|R_{02,mn}|$ and $|T_{02,mn}|$, as functions of normalized crack length, L, in a steel pipe: $H/R = 0.135$, $v = 0.287$, $D = 0.55$, and $f = 70$ kHz.

It can be seen from Eqs. (4.12)–(4.21) that all the matrices need be computed only for the first radius pair. In other words, the circumferential discretization does not affect the size of the matrices and, hence, the computational time. The problem is reduced now to a quasi-one-dimensional form.

When $q_C = q$, then $q_N = 0$. This situation corresponds to the axisymmetric crack. Then it is obvious that $\mu_{C,m_1m_2} = 0$ when $m_1 \neq m_2$, $\mu_{N,m_1m_2} = 0$ for all m_1 and m_2, and $\mu_{C,mm} = q$. Therefore, matrices $\left(H_C^R\right)^* G_C^R$ and $\left(H_N^R\right)^* G_N^R$ are reduced to diagonal block matrices. Furthermore, $\left(H_C^R\right)^* S_C^I$ and $\left(H_N^R\right)^* S_N^I$ in Eqs. (4.14) and (4.15) become null vectors. However, the kth block vector remains unchanged. Consequently, the problem becomes smaller in dimension and only the wave modes related to the incident circumferential wave number k need be considered. In this situation, it is easily shown that the subdivision in the circumferential direction does not add complexity to the numerical procedure because the parameter q is eliminated from the final linear equation.

Table 1
Laminated composite cylinder's material properties (C_{ij} in GPa) (0° is the z-direction)

Lamina	C_{11}	C_{12}	C_{13}	C_{33}	C_{44}	ρ (g/cm^3)
0° Inside	13.92	6.92	6.44	160.73	7.07	1.8
90° Outside	13.92	6.44	6.92	13.92	7.07	1.8

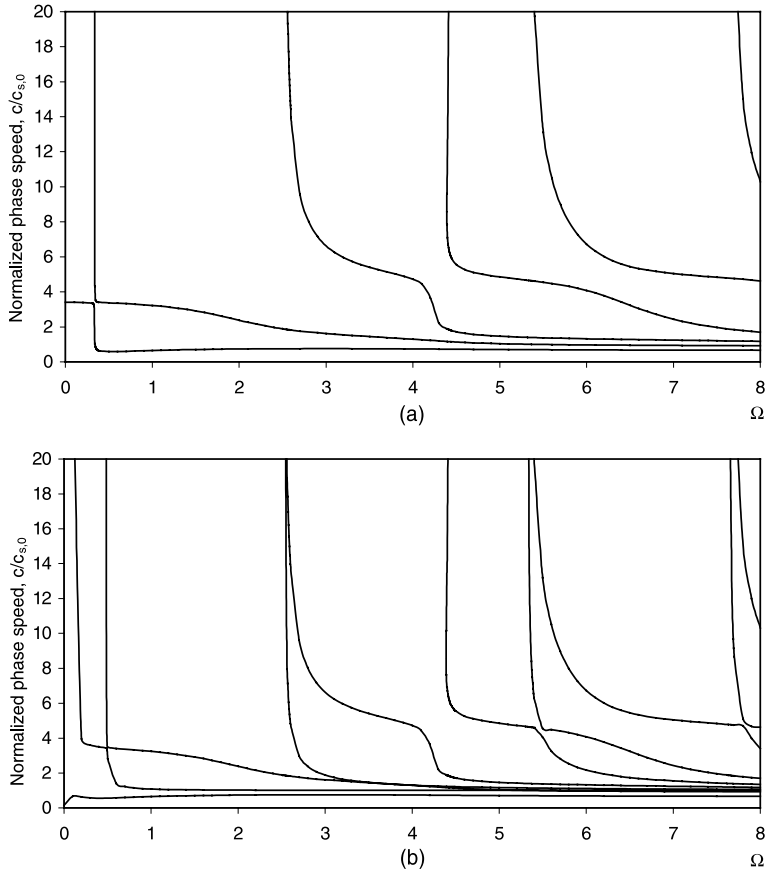

Fig. 4. Normalized phase speed versus frequency for a 2-ply [0/90] graphite/epoxy cylinder with $H/R = 0.1$ and (a) $m = 0$, (b) $m = 1$.

Once the linear equation (3.16) is established, the reflection coefficients for the symmetric case can be obtained. The solution for the anti-symmetric case can be found similarly. If the solutions of these two cases are known, the reflection and transmission coefficients, $R_{kl,mn}$ and $T_{kl,mn}$, for the problem considered are derived easily as

$$R_{kl,mn} = \frac{a^{\mathrm{S}}_{kl,mn} + a^{\mathrm{A}}_{kl,mn}}{2a^{\mathrm{I}}_{kl}}, \qquad T_{kl,mn} = \frac{a^{\mathrm{S}}_{kl,mn} - a^{\mathrm{A}}_{kl,mn}}{2a^{\mathrm{I}}_{kl}}, \tag{4.22}$$

where $a^{\mathrm{S}}_{kl,mn}$ and $a^{\mathrm{A}}_{kl,mn}$ represent the solutions for the symmetric and anti-symmetric cases, respectively. The numerical accuracy of the coefficients is checked by using the principle of energy conservation. The energy flux associated with each propagating mode has been discussed in Rattanawangcharoen et al. (1994).

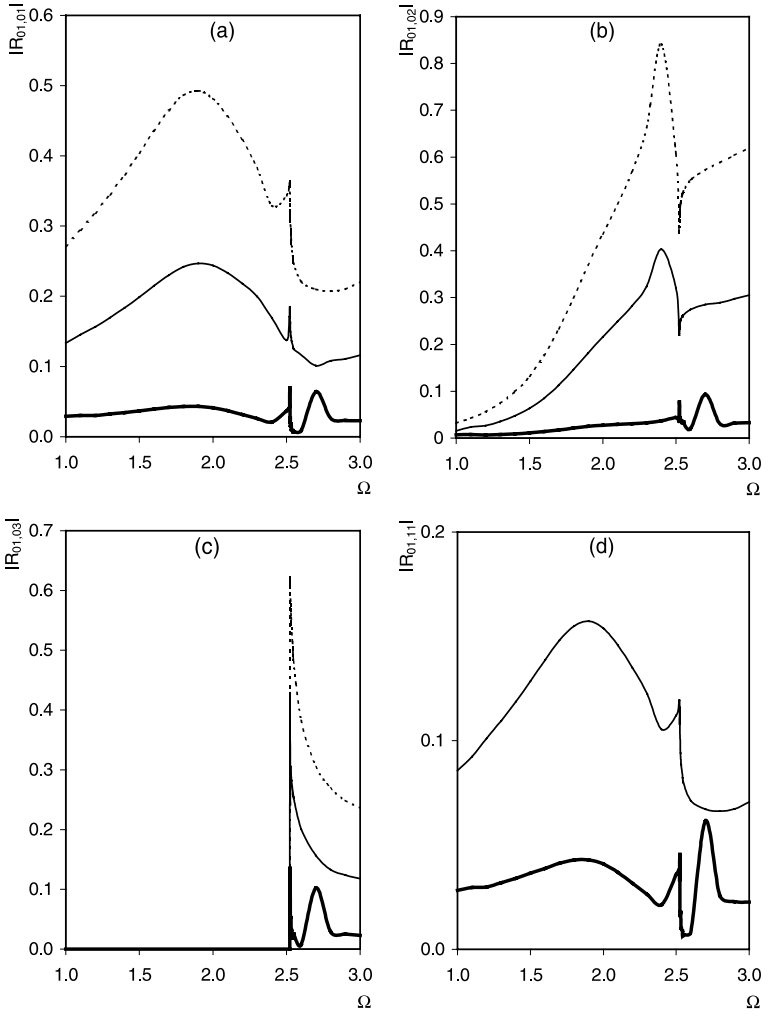

Fig. 5. Variation of reflection coefficients with different Ω for three normalized crack lengths $L = 0.1$ (——), $L = 0.5$ (——), $L = 1.0$ (- - -), in a 2-ply [0/90] graphite/epoxy cylinder. $H/R = 0.1$, $D = 0.5$, and (a) $|R_{01,01}|$, (b) $|R_{01,02}|$, (c) $|R_{01,03}|$, (d) $|R_{01,11}|$, (e) $|R_{01,12}|$, (f) $|R_{01,13}|$, (g) $|R_{01,14}|$, and (h) $|R_{01,15}|$.

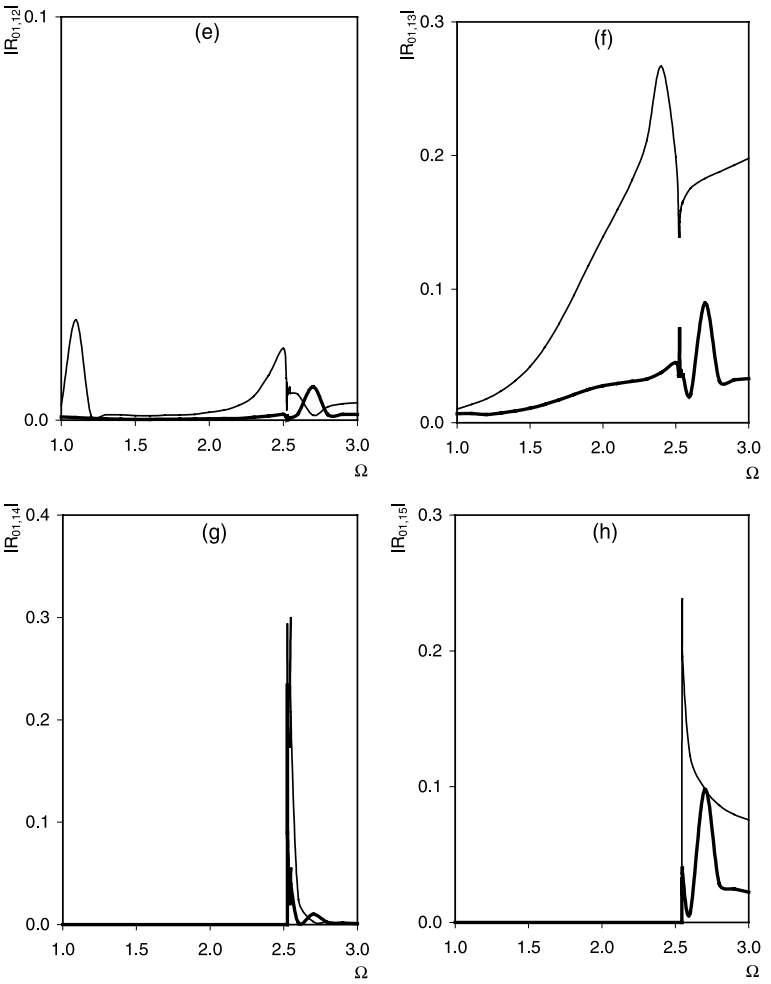

Fig. 5 (*continued*)

3. Numerical results and discussion

The previously described method can be used to analyze the effect of a planar crack located in a cross-section of the cylinder. The crack can have an arbitrary angle, θ_0, in the circumferential direction and an arbitrary depth, d, in the radial direction (see Figs. 1 and 2). To demonstrate the effectiveness and versatility of the proposed method, the following two illustrative examples are considered:

1. a homogeneous isotropic hollow cylinder; and
2. a 2-ply [0/90] graphite/epoxy hollow cylinder.

In both examples, H and R are the total thickness and mean radius of the cylinder, respectively. A normalized frequency, Ω, and normalized wave number, γ, are defined as,

$$\Omega = \frac{\omega}{\omega_{\text{ref}}}, \qquad \gamma = \frac{\xi}{\xi_{\text{ref}}},$$

where ω_{ref} and ξ_{ref} are the reference frequency and reference wave number, respectively. Furthermore, the results are presented for a normalized crack length, $L = R\theta_0/2\pi R$ and a normalized crack depth, $D = d/H$.

The total number of sublayers N_{sl} (or p) used in computing the discrete wave functions, the total circumferential wave number M, and the corresponding axial wave number N_m for each m $(-M \leqslant m \leqslant M)$ used in the wave function expansion are chosen to assure accuracy. The choice of these values is such that the coefficients in Eq. (2.1) converge and energy conservation is satisfied.

Example 1. This example is used solely to validate the present numerical procedure. The reflection of the second, essentially non-dispersive axisymmetric wave $L(0,2)$ is considered in a hollow cylinder. Poisson's ratio, ν, is taken to be 0.287, the thickness over the mean radius, H/R, is chosen as 0.135 and Young's modulus is 216.9 GPa. The crack length is 50% of the circumferential length and the crack depth is 55% of the thickness. The reference frequency and wave number are,

$$\omega_{\text{ref}} = \frac{1}{H}\sqrt{\frac{\mu}{\rho}}, \qquad \xi_{\text{ref}} = \frac{1}{H},$$

where μ is the shear modulus and ρ is the mass density of steel. The material constants correspond to the longitudinal and torsional wave velocities that are given, respectively, by

$$c_1 = 5.96 \times 10^3 \text{ m/s}, \qquad c_2 = 3.26 \times 10^3 \text{ m/s}.$$

Moreover, 20 sublayers and 23 circumferential wave numbers ($M = 11$) with $N_0 = 48$, $N_m = 41$ $(1 \leqslant |m| \leqslant 11)$ are employed.

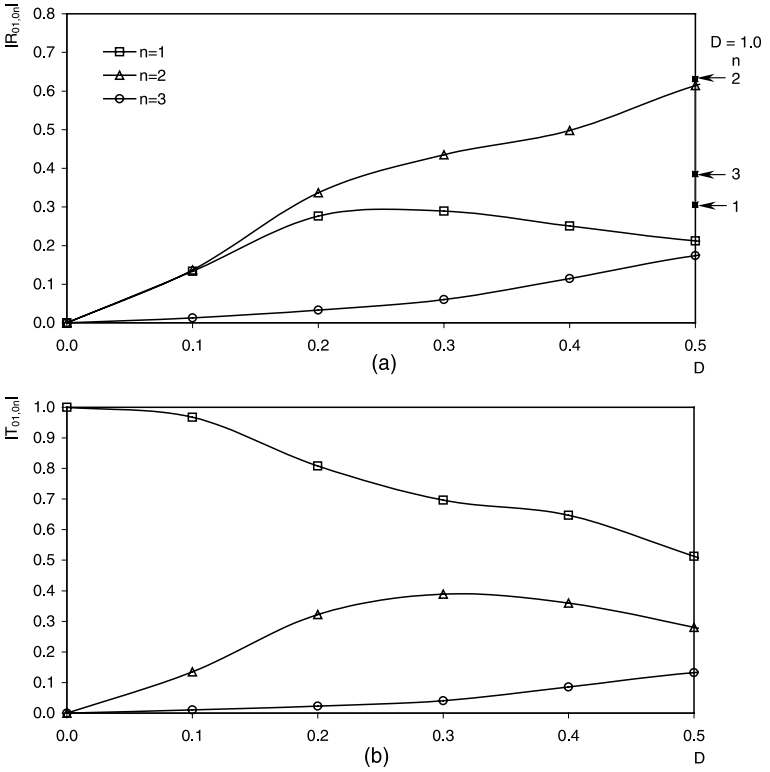

Fig. 6. Reflection and transmission coefficients, $|R_{01,0n}|$ and $|T_{01,0n}|$, as functions of normalized crack depth, D, in a 2-ply [0/90] graphite/epoxy cylinder at $\Omega = 3.0$: $H/R = 0.1$, and $L = 1.0$.

This particular problem was investigated experimentally and numerically by Alleyne et al. (1998) and by Lowe et al. (1998). The inner radius, R_i, and thickness, H, of the pipe are invariably,

$$R_i = 38 \text{ mm}, \qquad H = 5.5 \text{ mm}.$$

Fig. 3 shows the computed normalized reflection and transmission coefficients in comparison to those of Bai et al. (2001) who used exact wave functions. Such analytical expressions do not generally exist, however, so that the analogous results obtained here are determined by using a semi-analytical finite element approximation. Regardless, agreement between the two sets of computed data and the experimental results is always close in Fig. 3(a). Furthermore this figure has the interesting feature that $|\mathbf{R}_{02,mn}|$ and $|\mathbf{T}_{02,mn}|$, $m = 0$, $n = 1, 2$, are invariably linear functions of the length, L, of the crack. Such a simple relationship should enable L to be found more readily from these particular coefficients.

The second example considered is a composite cylinder.

Example 2. The scattering of an incoming propagating wave is also considered in a two-ply [0°/90°] graphite/epoxy cylinder. The thickness of each sublayer is taken to be equal, i.e. $H_1 = H_2 = 0.5$ so that $H = H_1 + H_2 = 1.0$. Elastic properties of each ply are listed in Table 1.

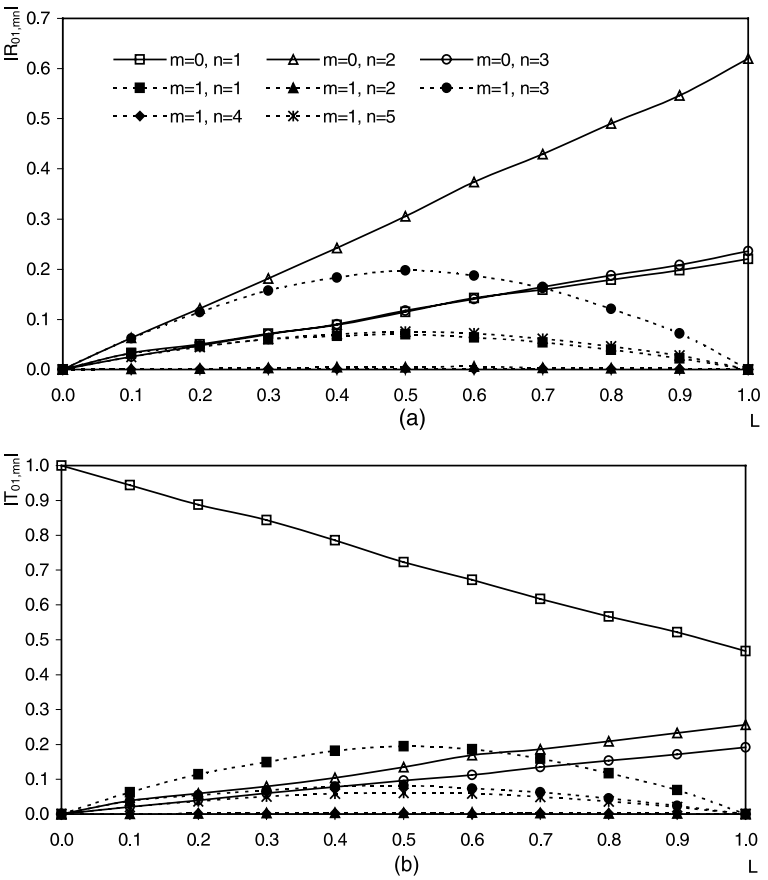

Fig. 7. Reflection and transmission coefficients, $|R_{01,mn}|$ and $|T_{01,mn}|$, as functions of normalized crack length, L, in a 2-ply [0/90] graphite/epoxy cylinder at $\Omega = 3.0$: $H/R = 0.1$, and $D = 0.5$.

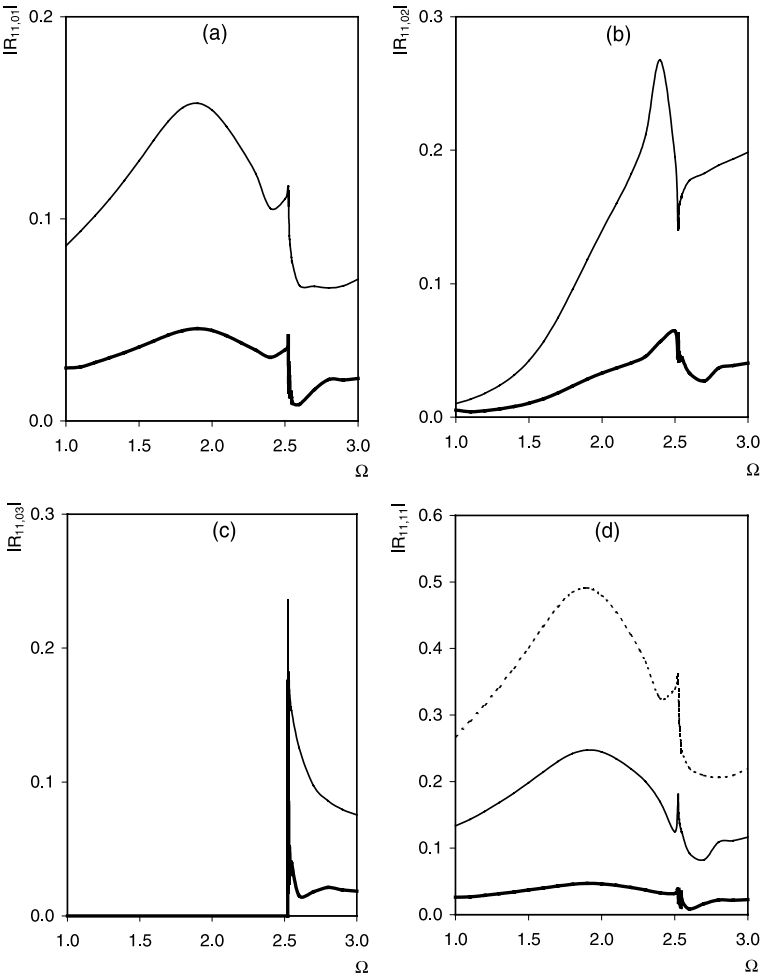

Fig. 8. Variation of reflection coefficients with different Ω for three normalized crack lengths, $L = 0.1$ (——), $L = 0.5$ (——), $L = 1.0$ (- - - -), in a 2-ply [0/90] graphite/epoxy cylinder. $H/R = 0.1$, $D = 0.5$, and (a) $|R_{11,01}|$, (b) $|R_{11,02}|$, (c) $|R_{11,03}|$, (d) $|R_{11,11}|$, (e) $|R_{11,12}|$, (f) $|R_{11,13}|$, (g) $|R_{11,14}|$, and (h) $|R_{11,15}|$.

The reference frequency and wave number are now,

$$\omega_{\text{ref}} = \frac{1}{H}\sqrt{\left(\frac{C_{55}}{\rho}\right)_{0^\circ}}, \qquad \xi_{\text{ref}} = \frac{1}{H}.$$

Moreover H/R is always 0.1 and the crack depth is invariably 50% of the thickness, i.e. the crack extends through the thickness of the 90° ply. On the other hand, the crack length is changed from 10% to 50% and 100% of the circumferential length. Note that, in the last case, the problem is axisymmetric so that only the $m = 0$ modes are excited.

Fig. 4 shows the phase velocity versus frequency in the range $1 \leqslant \Omega \leqslant 8$ for the corresponding uncracked cylinder. Numerical results for a cracked composite cylinder shown in Figs. 5 and 8, on the other hand, are restricted to $1 \leqslant \Omega \leqslant 3$ (i.e. the frequency-thickness product, fH, is between $0.3 \leqslant fH \leqslant 0.9$ mm/μs) in order

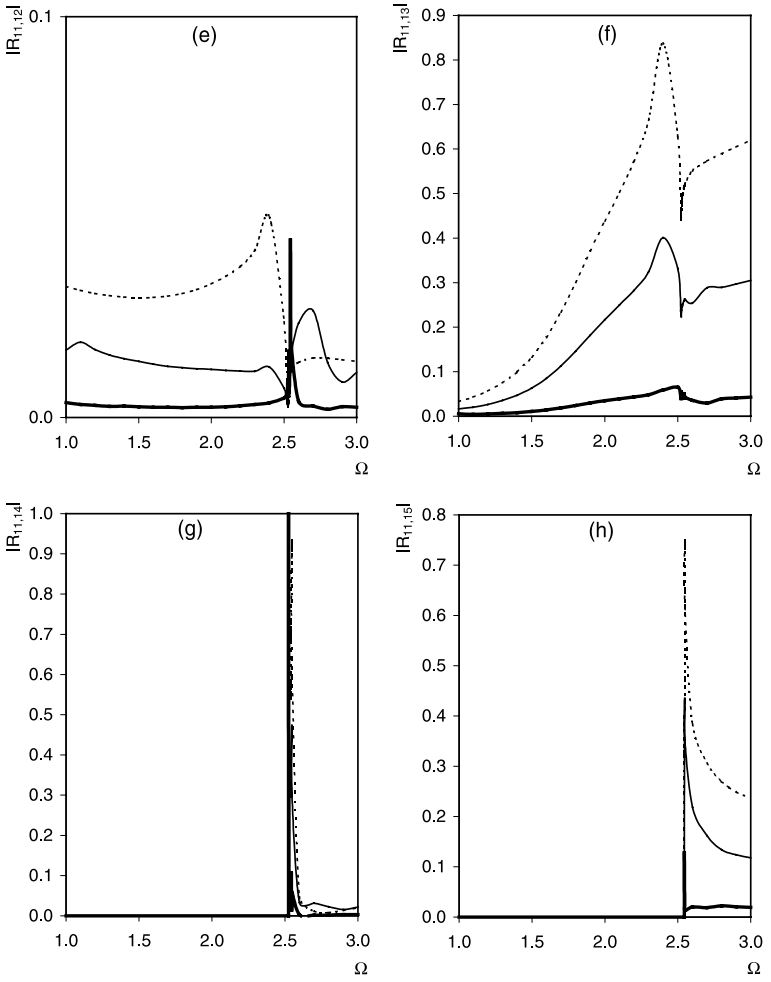

Fig. 8 (*continued*)

to limit the number of propagating modes. Indeed, if Ω is no greater than 3, Fig. 4 shows that there are only three and five propagating modes for $m = 0$ and 1, respectively. In addition, there are merely five propagating modes for $2 \leqslant m \leqslant 4$, and four propagating modes for $m = 5$. Moreover, for $m = 0$, the first cutoff frequency is $\Omega = 2.523$; for $m = 1$, the cutoff frequencies for the fourth and fifth modes are, respectively, 2.525 and 2.545 and, for $m = 2$, they are 2.531 and 2.600. It can be seen from Fig. 4 that the $L(0,1)$ and $F(1,1)$ modes are almost non-dispersive in the normalized frequency range $1 \leqslant \Omega \leqslant 3$ so that they are chosen as the incident wave modes in this example. After a preliminary check of the convergence of the reflection coefficients and energy conservation, 16 sublayers were employed to discretize a cracked cylinder in the radial direction and 23 circumferential wave numbers ($M = 11$) were used. For $m = 0$, $N_0 = 30$ was found to give good results. For $1 \leqslant |m| \leqslant 11$, it was necessary to employ $N_m = 43$.

Fig. 5 shows the reflection coefficients for different modes when the incident mode is $L(0,1)$. The figure indicates that sharp peaks occur for the reflection coefficients around the first cutoff frequency, $\Omega = 2.523$. When the excitation frequency is below this particular cutoff frequency, $|R_{01,01}|$ is more sensitive, at a given

Ω, to any one crack length than the other reflection coefficients shown. Conversely, $|R_{01,02}|$ becomes most sensitive to a crack when Ω is above the cutoff frequency. Clearly, the waves reflected from the crack involve not only the $m = 0$ modes, which correspond to the incident wave $m = 0$, $n = 1$, but also, due to mode conversions, the $m = 1$ modes. Overall, it appears that different circumferential crack lengths can be detected more readily if the $m = 0$, $n = 1$ and $m = 0$, $n = 2$ modes are used below and above the first cutoff frequency, respectively.

Fig. 6 presents the reflection and transmission coefficients for $\Omega = 3$ as functions of the crack depth, D, when the circumferential crack length is a constant $L = 1$ (i.e. axisymmetry holds). $|R_{01,02}|$ and $|T_{01,01}|$ show a characteristic monotonic increase and decrease with D, respectively. Conversely, $|R_{01,01}|$ and $|T_{01,02}|$ each have maxima around D = 0.3. On the whole, $|R_{01,02}|$ and $|T_{01,01}|$ are most sensitive to changes in D.

Fig. 7 gives the reflection and transmission coefficients as the crack length increases for $D = 0.5$. It is seen that the reflection coefficients $|R_{01,0n}|$, $n = 1, 2, 3$, increase linearly with the crack length L, which is a similar behavior to that found for the isotropic steel cylinder. Moreover $|R_{01,02}|$ and $|T_{01,01}|$ again dominate the reflected and transmitted fields, respectively, when $\Omega = 3$.

Results for the $F(1,1)$ rather than the $L(0,1)$ incident mode are shown in Figs. 8–10. The sharp peak at the first cutoff frequency, $\Omega = 2.523$, is clearly noticeable again in Fig. 8. Moreover, observations noted previously for $|R_{01,01}|$ can be made from Figs. 9 and 10 for the analogous $|R_{11,11}|$. However, those made for $|R_{01,02}|$ surprisingly pertain now to $|R_{11,13}|$ rather than $|R_{11,12}|$. Therefore straightforward extrapolations are not always applicable when interchanging the $L(0,1)$ and $F(1,1)$ incident waves.

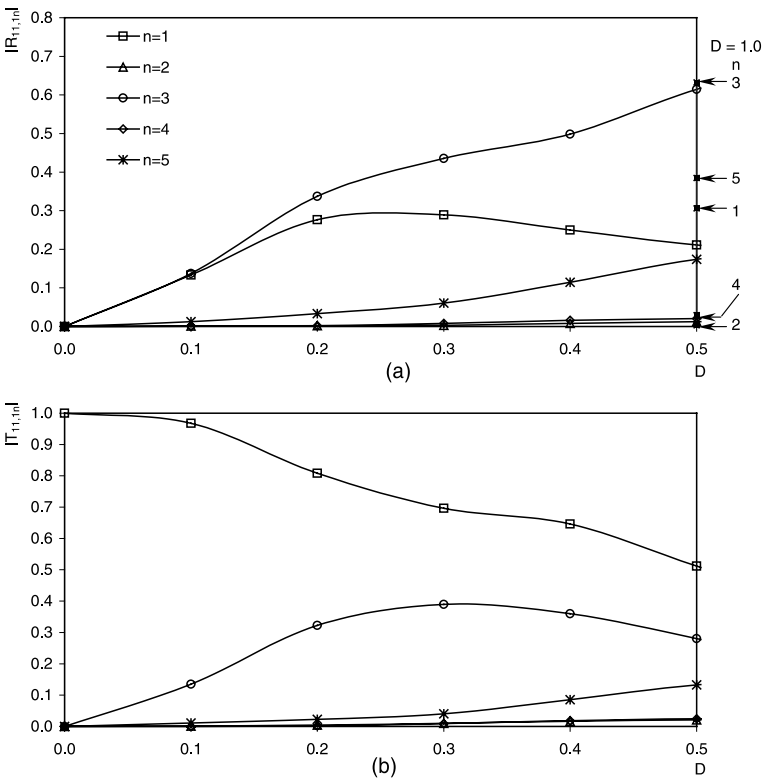

Fig. 9. Reflection and transmission coefficients, $|R_{11,1n}|$ and $|T_{11,1n}|$, as functions of normalized crack depth, D, in a 2-ply [0/90] graphite/epoxy cylinder at $\Omega = 3.0$: $H/R = 0.1$, and $L = 1.0$.

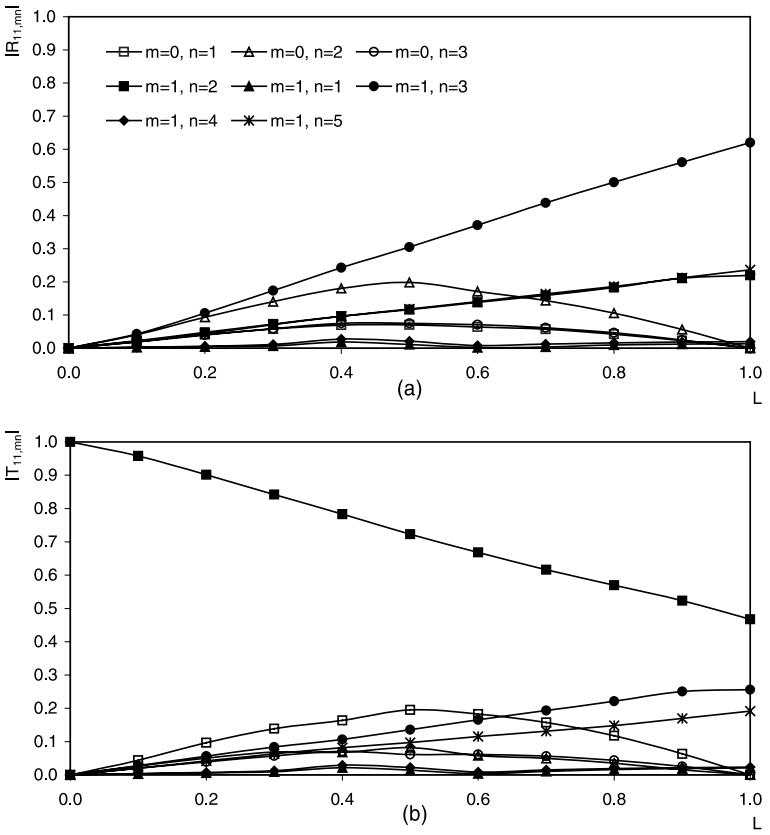

Fig. 10. Reflection and transmission coefficients, $|R_{11,mn}|$ and $|T_{11,mn}|$, as functions of normalized crack length, L, in a 2-ply [0/90] graphite/epoxy cylinder at $\Omega = 3.0$: $H/R = 0.1$, and $D = 0.5$.

4. Conclusions

A numerical procedure to efficiently represent a planar, circumferential crack in an isotropic cylinder has been extended to a cylindrically orthotropic material with little computational or error penalties. A virtually non-dispersive mode is chosen as an incident wave whose scattering may be used to detect or dimension a crack. The numerical results presented here confirm that the choice and frequency of such a wave is important because different incident waves produce a dissimilar pattern of mode conversions.

Acknowledgements

The first author would like to acknowledge the financial support from the University of Manitoba through a graduate fellowship award. AHS and NP would like to acknowledge the financial support of the Natural Science of Engineering Research Council of Canada. SKD would like to acknowledge the support provided by the Engineering Research Program, Office of Basic Energy Sciences, U.S. Department of Energy (DE-FG03-97ER14738).

References

Alleyne, D.N., Lowe, M.J.S., Cawley, P., 1998. The reflection of guided waves from circumferential notches in pipes. ASME Journal of Applied Mechanics 65, 635–641.

Bai, H., Shah, A.H., Popplewell, N., Datta, S.K., 2001. Scattering of guided waves by circumferential cracks in steel pipes. ASME Journal of Applied Mechanics 68, 619–631.

Bathe, K.J., 1982. Finite Element Procedures in Engineering Analysis. Prentice-Hall Inc, Englewood Cliffs, New York.

Datta, S.K., 2000. Wave propagation in composite plates and shells. In: Chou, T.W. (Ed.), Comprehensive Composite Materials, vol. 1. Elsevier, Oxford (Chapter 18).

Huang, K.H., Dong, S.B., 1984. Propagating waves and edge vibrations in anisotropic composite cylinder. Journal of Sound and Vibration 96 (3), 635–641.

Kohl, T., Datta, S.K., Shah, A.H., 1992. Axially symmetric pulse propagation in semi-infinite hollow cylinders. AIAA Journal 30, 1617–1624.

Lowe, M.J.S., Alleyne, D.N., Cawley, P., 1998. The mode conversion of a guided wave by a part—circumferential notch in a pipe. ASME Journal of Applied Mechanics 65, 649–656.

Pan, E., Rogers, J., Datta, S.K., Shah, A.H., 1999. Mode selection of guided waves for ultrasonic inspection of gas pipelines with thick coating. Mechanics of Materials 31, 165–174.

Rattanawangcharoen, N., 1993. Propagation and Scattering of Elastic Waves in Laminated Circular Cylinders. Ph.D. thesis, University of Manitoba, Winnipeg, Canada.

Rattanawangcharoen, N., Shah, A.H., Datta, S.K., 1994. Reflection of waves at the free edge of a laminated circular cylinder. ASME Journal of Applied Mechanics 61, 323–329.

Rattanawangcharoen, N., Zhuang, W., Shah, A.H., Datta, S.K., 1997. Axisymmetric guided waves in jointed laminated cylinders. ASCE Journal of Engineering Mechanics 123, 1020–1026.

Zhuang, W., Shah, A.H., Datta, S.K., 1997. Axisymmetric guided wave scattering by cracks in welded steel pipes. ASME Journal of Pressure Vessel Technology 19, 401–406.

Zhuang, W., Shah, A.H., Dong, S.B., 1999. Elastodynamic Green's function for laminated anisotropic circular cylinders. ASME Journal of Applied Mechanics 66, 665–674.